Multi-objective Optimisation and Multi-criteria Decision Making in SLS Using Evolutionary Approaches

Nikhil Padhye, Subodh Kalia and Kalyanmoy Deb
npdhye@gmail.com, subodh@iitk.ac.in, deb@iitk.ac.in
Department of Mechanical Engineering
Indian Institute of Technology Kanpur, Kanpur-208016, U.P., India
KanGAL Report 2009008

December 24, 2009

Abstract

This paper proposes an integrated approach to arrive at optimal build orientations, simultaneously minimizing surface roughness '*Ra*' and build time '*T*', for object manufacturing in SLS process. The optimization task is carried out by two popularly known multi-objective evolutionary optimizers - NSGA-II (non-dominated sorting genetic algorithm) and MOPSO (multi-objective particle swarm optimizer). The performance comparison of these two optimizers, along with an approximation of Pareto-optimal front is done using two statistically significant performance measures. Three proposals addressing the task of decision making, i.e. selecting one solution in presence of multiple trade-off solutions, are made to facilitate the designer. A hill climbing local search procedure is also proposed to further refine the solutions obtained by evolutionary optimizers. The overall procedure is integerated into a *MORPE* - Multi-objective Rapid Prototyping Engine. Several sample objects are considered for experimentation to demonstrate the working of *MORPE*. A careful study of optimal build directions for several components indicates a trend, providing insight into the SLS processes which can be regarded highly useful for various practical RP applications. Multi-objective Optimization, Decision Making, Genetic Algorithms, Particle Swarm Optimization and SLS.

1 Introduction

Rapid prototyping (RP) or layered manufacturing refers to processes in which a component is fabricated by layer-by-layer deposition of material from 3D computer asisted design models. RP is playing an important role in reducing the time required for new product development and lowering development costs, thus many companies are realizing the benefits of producing prototypes quickly and easily. Today there exist multiple RP techniques. Common examples of RP techniques are Fused Deposition Method (FDM), Stereolithography (SLA), Selective Laser Sintering (SLS), Laminated Object Manufacturing (LOM), 3D printing and Direct Metal Deposition (DMD). With the advent of these technologies, it is now possible to fabricate physical prototypes directly from CAD models for checking the feasibility of design concept and prototype verification.

SLS process is one such most popular RP processes for object manufacturing [15]. Rapid growth of SLS can be attributed to its ability to process various materials like polymers, metals, ceramics and composites. Commercial SLS systems (such as EOS P 380) build the parts by selective solidification of the thermoplastic polymer powder by CO_2 laser. First, tessellated CAD model is sliced with layer thickness ranging from 0.1 to 0.3 mm. Powder is spread on the machine bed with help of a re-coater. The powder is pre-heated to about $4-5^{\circ}$ C below its melting point to keep the amount of energy contributed by laser as low as possible. This is done by means of four heat radiators present in the built chamber. The laser sinters

the powder and leads to a local solidification of the material. In the sintering process the temperature of the powder is raised to a point of fusing without actual melting. After allowing sufficient time for the sintered layer to cool down without causing significant internal stresses, the part bed moves down by one layer thickness and powder is again spread by the re-coater. The sintered material forms the part while the un-sintered powder remains in its place to support the structure and is cleaned away once the build is complete. This process is repeated and prototype gets created.

The quality of the prototype is usually characterized by its surface roughness, accuracy and strength. While cost of fabrication is directly related to build time [6]. To achieve better accuracy or enhanced surface finish deposition of finer slices is desired. Such a deposition is likely to increase build time. Thus, there is always a conflict between two simultaneosly considered goals of achieving better surface quality and reducing the build time. However; appropriate selection of build orientation can help acheiving these goals simultaneously.

Since appropriate build directions are unknown a search to identify favorable orientations which simultaneosly minimize *Ra* and *T* is needed. The minimization of two conflicting objectives leads to set of trade-off solutions with varying *Ra* and *T* corresponding to a set of build orientations. From a designers point an optimal orientation needs to be chosen for final fabrication, putting forward the issue of 'Decision Making'. Much of past work has focussed on finding optimal build orientations in different RP processes but 'Decision Making', atleast to best knowledge of the authors, has not received any major attention. To tackle this issue, this paper proposes three 'Decision Making' schemes while demonstrating their working on sample objects. Post optimal analyses on various sample objects is also carried out revealing additional information which can be regarded highly useful from a practical stand-point. The entire procedure is automated using a developed software - *Multi-objective Rapid Prototyping Engine* (*MORPE*) to achieve aformentioned task. The software tool is used for SLS system and is easily modifiable for other RP techniques. *MORPE* incorporates two multi-objective evolutionary algorithms (MOEAs), NSGA-II and MOPSO, for optimization purposes, inbuilt performance measures, like attainment surface estimater and hypervolume calculator to arrive at results of statistical importance, 'Local Search' procedure to improve upon the solutions obtained from MOEAs and 'Decision Making' schemes to facilitate the designer to select an optimum fabrication orientation. This tool is made freely downloadable from http://home.iitk.ac.in/∼npadhye and should serve as useful resource for entire RP community.

Rest of the paper is structured as follows. Section 2 reviews LM literature for studies related to optimal build orientation. In section 3 the multi-objective problem formulation in context to SLS process is set up. This is followed by section 4 which systematically proposes an approach to address the task of arriving at optimal build orientations. This section briefly introduces two multi-objective evolutionary optimizers (NSGA-II and MOPSO). Then, introduction to stastically comparable performance measures, *Hypervolume Indicator* and *Attainment Surface Approximator*, is made. Finally, the section describes a proposed mutation driven hill climbing local search using achievement scalarizing function (ASF) for refinement of solutions obtained by evolutionary optimizers. In section 6 several solid models from simple to complicated geometries are considered for bi-objective optimization to investigate and valid the working of *MORPE*. Results and discussions on the experiments are presented in section 7 and inferences are drawn. This section also provides insight into the decision making issue and innovative design principles are deciphered via. post optimal analysis. Finally, section 8 summarizes the major findings in this study with major conclusions.

2 RELATED WORKS

There has been a keen interest in build orientation studies for part fabrication in LM manufacturing for more than a decade. Various goals, like surface finish, build time, support structure etc. have been considered for different processes in past. Apart from the dependance on build orientations, these goals largely behave in accordance with the specific LM technology and hence optimum orientations for one process might not be optimum for another process. Thus, once the measure(s) to quantify these goals is decided a

search procedure is required to identify the favorable orientations for specific RP process. Following paragraphs chronologically summarize various attempts in this direction and help us to compare and identify shortcomings in past approaches.

In [10] the authors proposed an interactive system to decide a suitable part orientation. Here surface roughness was treated as primary objective and build time as secondary objective, and thus guidelines were formulated based on experience. In [5] a multi-objective approach is attempted for SL parts by considering dimensional accuracy and build times as objectives. The part accuracy was treated as the primary objective and was calculated based on experience for different types of surfaces. The second objective considered for minimization was build time (quantified by number of slices). This work also introduced adaptive slicing based on pre-specified cusp height. The orientation selection was made in two steps: firstly few orientations based on part-accuracy were shortlisted and then a 'best' orientation was found based on build time as criterion.

In [16] part orientation for SL parts was determined based on considerations of surface quality, build time or the complexity of the support structures. Surface quality was attained either by maximizing the area of non-stepped surfaces or by minimizing the area of worst quality surfaces. Build time was estimated indirectly as part height in build direction. Support structure was minimized by minimizing the number of supported points. Suitable orientation for one of the objectives at a time was determined from the list of preselected base planes.

In [9] proposed a system to compute part orientations for SL parts, obtaining a trade-off in time, cost and accuracy. The feature based tool considers cost, uild time, problematic features, optimally oriented features, overhanging areas and support volume for proposing build direction. The overall tool comprises of fowllowing modules: orientation, timing, cost, problematic feature and display. In orientation module one or more candidate orientations are chosen based on considerations of critical surfaces, holes, cuts, shafts, protusions, shell and axes. Then these orientations are evaluated on criteria of: overhanging area, volume of support structure, build time, cost of the part and problematic features. A total score is allocated based to each of pre-selected orientations based on above criteria. The orientation with maximum total score is finally selected.

In [18, 19] volumetric error minimization approach is adopted. Here, the difference between the volume of the part deposited using uniform slices and that of CAD model was minimized for determining orientation. This approach utilized primitive volume approach, which assumed a complex part to be constructed from a combination of basic primitive volumes. In laster study authors presented a generic approach in which tessellated CAD models were utilized instead of basic primitive shapes.

In [29] a process planning approach was proposed to improve build performance in SL by lowering build time, achieving better accuracy and high quality surface roughness. Process planning consisted of three modules: orientation, layer thickness and parameter selection. Part deposition orientation, layer thickness sweep period, z height, fill overcure and hatch over cure were chosen as the process variables and were decided based upon considerations of support structure and horizontal planes as the constraints. In the part orientation module a set of most feasible orientations were evaluated based on planar, conical and cylindrical surfaces present on the part. The part was oriented in these preselected orientations and sliced uniformly leading to trade-off in considered objectives. The four most suitable alternate orientations were selected for further investigations in slicing and parameter modules to end up with the most suitable process plan. In [11], from a set of preselected orientations, best orientation was decided which led to least number of adaptive slices.

In [28] a real coded genetic algorithm was employed to obtain optimal build orientation and single objective weighted approach was used to construct a single objective by combining average surface roughness and build time. Later, in [25] a bi-objective study was conducted, simultaneously minimizing surface roughness and build time, to find a set of trade-off solutions.

In [2], combined objective of average weighted surface roughness (AWSR) and build time, using fuzzy weights, is minimized by usage of a genetic algorithm. In [3] authors carried out a multi-criteria decision making approach with objectives of surface roughness, build time, and part cost. These objectives were

assigned a weight and combined into a single objective which was considered for minimization.

In [1] single objective genetic algorithm was again employed to determine optimal fabrication directions for LM processes so as to minimize the required post-machining region (RPMR) in LM (as post-machining is often required to improve the surface quality). Here, the authors developed an expression of the distribution of surface roughness and relation between the RPMR and fabrication direction.

In [4] build orientations for parts fabricated with stereolithography are derived for optimizing build time, surface roughness and post-processing times using single objective weighted approach. Other studies in literature that have also employed single objective weighted approach are [13, 30].

Irrespective of the objective(s) considered for determining build orientation, pre-selection of orientations or minimization of weighted single objective function, as done in earlier studies has well-known defficiencies and optimality of the solutions cannot be gauranteed [7]. However, more recently suitable multi-objective optimization approaches using genetic algorithms, i.e. simultaneously minimizing or maximizing multiple goals, have been studied for different LM processes [17, 23, 24, 25, 26]. Similar attempts to optimize multiple goals in this direction have been made [12, 31, 32, 33]. Despite such studies, systematic application of nature inspired huerestics coherently addressing multi-objective optimization, decision-making and knowledge discovery through optimization is still missing. To address the existing shortcomings we have chosen SLS process for which optimal build orientations are determined.

3 MULTI-OBJECTIVE PROBLEM

Without loss of generality, we assume that the goal is to minimize m functions $f_1, \ldots, f_m$ of n-dimensional decision variables ϕ. A decision vector $\phi_1 \in S$ is called Pareto-optimal if there is no other decision vector $\phi_2 \in S$ that dominates it. Any vector ϕ_1 is said to dominate ϕ_2 if ϕ_1 is not worse than ϕ_2 in all of the objectives and it is strictly better than ϕ_2 in at least one objective. In case two solutions ϕ_1 and ϕ_2 do not dominate each other, we say that they are indifferent to each other or are non-dominated with respect to each other. To solve such problems, algorithms which can find a well distributed set of trade-off and well converged set of solutions with least computational expense are desired.

In current study the objectives of interest are average surface roughness $\bar{Ra}$ and total build time T. Thus, the following bi-objective optimization can be set up.

Minimize $f_1 = \mathrm{Ra}(\phi)$

Minimize $f_2 = \mathrm{T}(\phi)$

with: $\phi = \{\theta_x, \theta_y\}$

subject to:
$0 \leq \theta_x \leq 180$
$0 \leq \theta_y \leq 180$

The problem variables are $\theta_x and \theta_y$ representing the rotations from an initial configuration about some reference XYZ Cartesian coordinate system. Figures 3(a) and 3(b) describe the rotation scheme stated here by considering rotation of a facet or planar triangle (CAD model represented in form of facets can be rotated by rotation of all facets). Computation of surface roughness Ra and build time T has been borrowed from [27] and briefly described as follows:

3.1 Surface Roughness

where for SLS surface roughness (in micrometers) is calculated differently for *up facing* and *down facing* surfaces as follows:

$$Ra_{up} = -2.04067 + .22\alpha + 0.06722t - 0.001368\alpha^2 \quad (1)$$

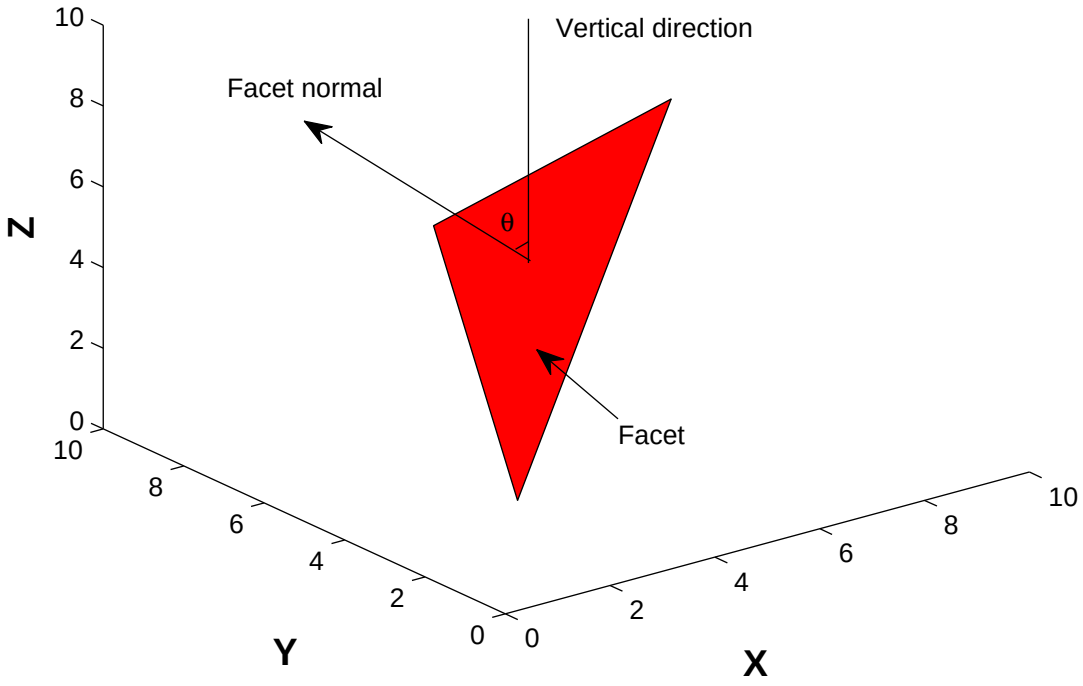

Figure 1: Build angle for SLS

$$Ra_{down} = 185 - 9.52P - 0.834\alpha - 0.157t + 0.15P^2 - 0.00099\alpha^2 + 0.0058\alpha t \quad (2)$$

Angle $\alpha = 90^\circ - \theta$, where θ is the angle between vertical direction and facet normal as shown in Figure 1

Thus, average surface roughness of entire part can be calculated as:

$$Ra_{av} = \frac{\sum Ra_i A_i}{\sum A_i} \quad (3)$$

Where Ra_i and A_i are surface roughness and area of the i^{th} triangular facet of STL file. Ra_i is computed from equations (1) or (2).

3.2 Build Time

Build time (T) in RP processes can be calculated by taking the sum of the times taken to draw exterior contour, fill the interior area on a layer, generate support structures, and other non-productive times, such as platform motion and warming time in SLS. Usually non-productive times are independent of build orientation. In case of SLS, the major portion of the time is taken during re-coating of the powder. Since, SLS does not require any support structure no additional time is needed to build support. Therefore, by minimising the height of the part in the direction of deposition, build time can be minimised. If Z-axis denotes the build direction then build time estimate is given by object height as:

$$T = (Z_{max} - Z_{min}) \quad (4)$$

Other rotation schemes can also be adopted for this purpose, but since material laying deposition is assumed to be along Z-axis, the rotation about Z-axis is invariant for the computation of objective axis, hence, only X-axis and Y-axis rotations are considered.

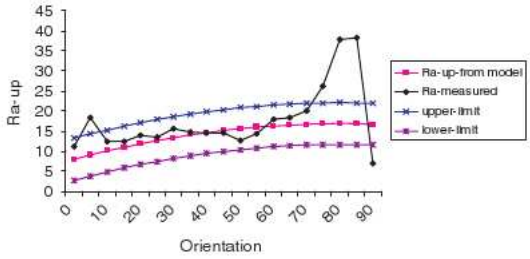

(a) *Ra*-up with respect to build angle.

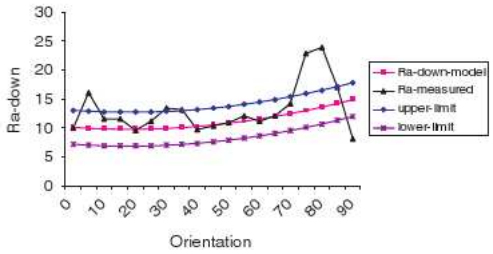

(b) *Ra*-down with respect to build angle.

Figure 2: Variation of *Ra*-up and *Ra*-down. **This figure has been copied, is it allowed, and what to cite.**

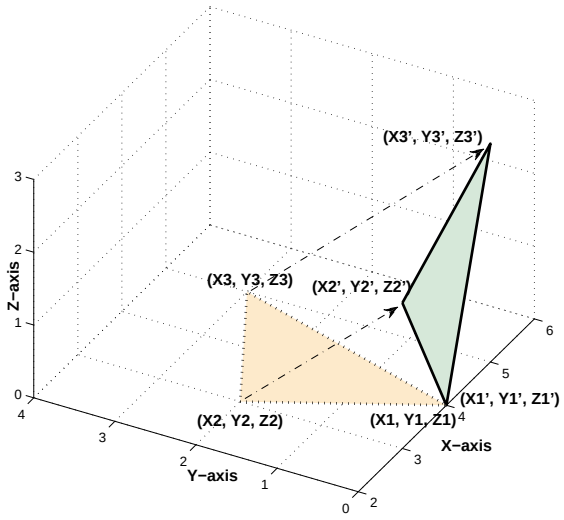

(a) Rotation of the facet about X axis by 90° with initial position (X_i, Y_i, Z_i) to final position (X'_i, Y'_i, Z'_i).

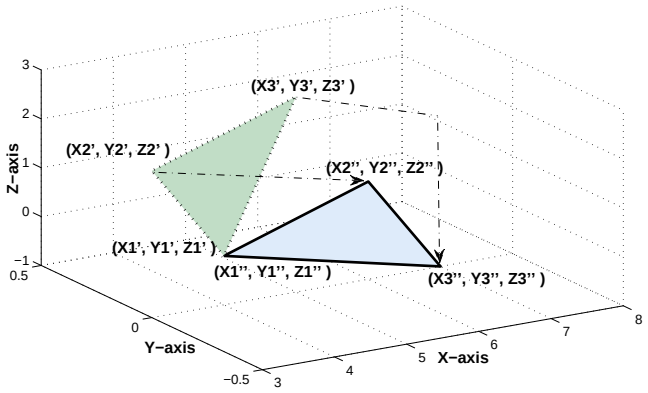

(b) Rotation of the facet about Y axis by 90° with initial position (X'_i, Y'_i, Z'_i) to final position (X''_i, Y''_i, Z''_i)

Figure 3:

4 PROPOSED APPROACH

The overall procedure is carried out by MORPE which comprises of following modules: a) Adaptive slicing procedure b) Multi-objective optimisers- NSGA-II and MOPSO c) Performance comparison tools-Hypervolume Indicator and Attainment Surface Approximator d) Local Search Tool e) Decision Making Kit. Figure 4 portrays the working of MORPE. For MORPE, Adaptive slicing procedure has been developed in Matlab version R2007a. The optimisation routines and performance comparison measures are developed in C (gcc version 4.3.2) language. Matlab code is compiled using MCR (matlab compiler runtime) version 7.6 and integrated with optimisation engine. The experiments reported in this study have been carried out on Intel single core 2.9 GHz, RAM-1.0 GB, Hard disk-80GB, OS-Linux-ubuntu-9.04, Computer architecture-32 bit. The codes developed in this paper can be obtained from following url http://home.iitk.ac.in/∼npadhye.

4.1 Evolutionary Optimisers

Although there exist several multi-objective evolutionary algorithms (MOEAs) in literature, popularly used genetic algorithm based NSGA-II and particle swarm based MOPSO optimisers have been utilised in this study. In the following paragraphs we briefly describe the working and salient features of these algorithms.

MOPSO: Particle swarm optimisation (PSO) is now a well established optimisation technique. PSO is a population based technique, similar in some respects to other evolutionary algorithms, except that potential solutions (particles) move rather than evolve through the search space. More recently, PSO has successfully been extended to multi-objective optimisation problems and such methods are called Multi-objective Particle Swarm Optimisation (MOPSO). PSO consists of several candidate solutions called particles each of which has a position and velocity, and experiences linear spring-like attractions towards two attractors:

1) the best position attained by that particle so far (particle attractor or personal best - *pbest*);

2) the best of the particle attractors in a certain neighbourhood (neighbourhood attractor or global best - *gbest*).

In each generation or cycle ('t'), every individual is associated with a position vector ($\bar{\phi_t}$) and a velocity vector ($\bar{v_t}$). The size of these vectors is equal to the number of decision variables in the problem. The position and velocity of each individual is updated according to following equations:

$$\bar{v_t} = w\bar{v_t} + c_1\bar{r_1} \cdot (\bar{PBest_t} - \bar{\phi_t}) + c_2\bar{r_2} \cdot (\bar{GBest_t} - \bar{\phi_t}) \tag{5}$$

$$\bar{\phi_{t+1}} = \bar{v_t} + \bar{\phi_t} \tag{6}$$

Equations (5) and (6) indicate position and velocity updates. The term w is known as inertia weight and, c_1 and c_2 are known as learning factors. In our procedure w has been chosen as 0.5, c_1 and c_2 are both taken to be 1.0. To preserve diversity in the population often random disturbance, called "turbulence", is added stochastically to a particle's position.

The MOPSO utilized in this study has been borrowed from [22, 21]. Table 1 summarizes the outline of MOPSO. Complete details on MOPSO can be found in [22]. The major difference in MOPSO and PSO is in the notion of defining 'Pbest' and 'Gbest' as there are more than one objectives under consideration in MOPSO. In this study, *NWtd.* and *Dom.* methods have been chosen for personal best and global best selections. For more details on guide selection reader is referred to [22], [20].

NSGA-II: Elitist Non-Dominated Sorting Genetic Algorithm (NSGA-II) is one of the most popularly used GA for multi-objective optimization. Several salient features like elite preservation and explicit diversity preserving mechanisms ensure its good convergence and diversity. Brief description of NSGA-II procedure is presented here, for further details reader is referred to [7, 8]: In NSGA-II, Figure 5, offspring population (size N) is created by using parent population (size N) by usual genetic operators: selection, crossover and mutation. The created child population is combined with parent population, to form combined population of size 2N, and then a non-dominated sorting is carried out to classify the entire population into several non-dominated fronts. The new population (size N) is then filled by the members of combined population belonging to different non-dominated levels or starting from first level. Since all members of combined population cannot be accomodated in new population - several non-dominated fronts have to discarded. Since all members of last front entering the new population may not be accommodated, only few members (corresponding to number of available slots) are selected from the last front based on the crowding distance technique. Binary tournament selection, SBX, and polynomial mutation operators are used for NSGA-II.

Table 1: MOPSO algorithm

MOPSO Algorithm
BEGIN
t=0
Initialise population P_t :
For i = 1 to N
Initialise $\bar{\theta}_t^i$, $\vec{v}_t^i=\bar{0}$ and $PBest_t^i=\{\bar{\theta}_t^i\}$ i.e. $\vec{p}_t^i=\bar{\theta}_t^i$
End
Initialise GlobalBest i.e. $GBest_t$:={}
Do
Evaluate (P_t)
$GBest_{t+1}$:= *Update*($P_t, GBest_t$)
For i = 1 to N
$PBest_{t+1}^i$:= *Update*($\bar{\theta}_t^i, PBest_t^i$)
End
P_{t+1}:=*Generate*($P_t, GBest_t$)
For i = 1 to N
MoveParticle($\bar{\theta}_t^i$);
End
SQP($GBest_t$)
t = t + 1
While(t$\leq t_{max}$**)**
END

4.2 Performance Comparisions

Due to stochastic nature of evolutionary approaches, it is difficult to conclude anything about performance from just one simulation. To eliminate the random effects and gather results of statistical significance, we perform multiple (11) runs of the evolutionary algorithm corresponding to different initial seeds. Two performance measures commonly used in EA literature have been employed in this study as follows:

Attainment Surfaces: Multiple runs, corresponding to different initial seeds, of an evolutionary algorithm usually result in multiple non-dominated set. Thus, to deduce overall performance an approximation of best non-dominated set, also referred to as 1_{st} attainment surface, is computed from available non-dominated sets. Since non-dominated can be visualized easliy in two and three dimensions, such a method provides good insight into algorithms performance. The computation of attainment surfaces is done by using attainment surface package described in [14].

Hypervolume indicator: Hypervolume is a measurement which takes into account the diversity as well as the convergence of the solutions [34]. Hypervolume represents the sum of the areas enclosed within the hypercubes formed by the points on the non-dominated front and a chosen reference point. For minimization type problems a higher value of hypervolume is desirable, as it is indicative of better spread and convergence of solutions. Figure 6(a) illustrates hypervolume computation of a non-dominated points w.r.t. a reference point 'R'. It should be noted that contribution to hypervolume is only made by points which are dominated by the reference point. All points not dominated by the reference point have zero contribution to the hypervolume. In this study we have computed average hypervolume curves over several generations for study and comparisions purposes. Although, hypervolume computation is dependent on choice of reference point, yet it is regarded as a good measure and can be employed for higher number of objectives as well.

4.3 Local Search

Typically for any practical multi-objective optimization problem location of true Pareto-optimal solutions is unknown. Although, MOEAs provide a good means to reach approximate or close to Pareto-optimal solutions, often further improvement on obtained solutions is possible by conducting *local search*. Local search usually considers obtained non-dominated solution and tries to improve it by utilizing a construction of single objective function.

In this study we construct an achievement scalarizing function (ASF), a single objective function, and consider its minimization. Following describes ASF scheme:

Consider such a starting point **y** (having objective vector **f(y)** and **z**=**f(y)**), then ASF = :

$$\min_{x \in S \subset \mathbb{R}^n} \max_{i=1}^{M} \frac{f_i(x)-z_i}{f_i^{max}-f_i^{min}} + \rho \sum_{j=1}^{M} \frac{f_j(x)-z_j}{f_j^{max}-f_j^{min}}$$

Where **z=f(y)** is usually reffered to as a reference point for local search, and f_i^{max} and f_i^{min} are minimum objective values of the 'best non-dominated' set. By minimizing **ASF** solutions are projected on the Pareto-front and convergence can be garaunteed.

Although various single objective optimization techniques could be applied for minimizing ASF, but due to discontinuos nature of objective functions gradient based methods are not preferred. We employed SQP (Sequential Quadratic Programming) based local search for this purpose and no improvement was found. A mutation driven or hill climbing strategy, is proposed for this minimization task. Table 4.3 describes the hill climbing approach. To conduct local search a maximum number of trials (MaxTrials) are pre-set to limit the number of function evaluations. Then, with equal probability, problem variables θ_x and θ_y are perturbed according to gaussian distribution (mean 0.0 and standard deviation σ_i). Standard deviation (σ_i) for gaussian distribution is varied linearly from 10.0 to 1.0 over the iterations. Such a local search enables to explore wider regions in the starting and becomes more focussed towards the end. If ASF at newly created orientations is lowered, then the perturbations in θ_x and θ_y are accepted. The whole procedure is continued till termination criteria is met.

5 Decision Making

When a set of trade-off solutions is obtained from a multi-objective optimization exercise, a decision point needs to be chosen to proceed further. This is often a non-trivial task for an operator and certain guidelines are necessary. To address this task, we introduce three decision making techniques, namely- *'Aspiration Point Method'*, *'Marginal Utility Method'* and *'L_2 Metric Method'*. The first method requires an 'aspiration point', described later, as an input from the user. However; remaining two methods do not require any user input to arriveat the decision choice. These methods are described as follows:

Aspiration Method: Here it is assumed that the designer has some pre-decided preference (or aspiration) for an operating point with which he/she is likely to settle. The goal is to find a solution which is better than the aspiration of the designer. Thus, it is called an aspiration point method. To carry out the search we allocate this aspiration point as the reference for ASF scheme (described in section 4.3), and evaluate ASF for all points on the Pareto-optimal front. The Pareto-optimal solution which corresponds to lowest ASF value, w.r.t. reference point, is selected. In this study we have considered three aspiration points as follows:

$Asp_1 = (\frac{Ra_{min}+Ra_{max}}{2}, \frac{T_{min}+T_{max}}{2})$,

$Asp_2 = (\frac{Ra_{min}+Ra_{max}}{2}, T_{max})$,

Asp_3= (Ra_{max}, $\frac{T_{min}+T_{max}}{2}$)

The corresponding decision choices obtained on the Pareto-front are indicated as P_1, P_2 and P_3. Asp_1, for example, implies that user is willing to accept an available point in proximity of the mean of best and worst obtained (Ra, T) values. In case of convex Pareto-optimal decision choice dominates the aspiration point, whereas in case of concave set decision choice gets dominated by the aspiration point.

Marginal Utility Method: This approach also does not require any prior information the user and searches for a Pareto-optimal solution which shows least affinity towards any of its neighbours in objective space. To compute affinity, consider three non-dominated points P_1, P_0 and P_2, s.t. ($Ra_1 \leq Ra_0 \leq Ra_2$) and ($T_1 \geq T_0 \geq T_2$) and we are interested in evaluating the affinity at the middle point P_0. P_1 and P_2 lie in the neighbourhood of P_0 and are selected as follows: consider k points, $P_{0,m}$ m = 1 to k, nearest to P_0, with $Ra_{0,m} \leq Ra_0$. Then centroid of all $P_{0,m}$s is computed and a point out of $P_{0,m}$s, which is closest to the centriod, is selected as P_1. For selecting P_2, same excercise is repeated, but this time considering points s.t. $Ra_{0,m}$s are greater than Ra_0.

Once P_1 and P_2 are computed for P_0, *affinity function* (AF), is calculated as :

AF_{P_0}=max(W1,W2); W1= $\frac{Ra_{P_0}-Ra_{P_1}}{T_{P_1}-T_{P_0}}$ and W2= $\frac{Ra_{P_2}-Ra_{P_0}}{T_{P_0}-T_{P_2}}$.

For each point in the non-dominated set, except for k extreme points at both ends, AF is computed and the solution with minimum AF is assigned as decision choice. This solution is argued to posses least affinity to move away from. In this study value of k is taken equal to 6. The value of k decides the resolution of the proximity in which we are interested to compute the affinity function. Decision point point by this method is usually a *'knee point'*. *'Knee points'* are often of great practical importance as they denote a coordinate on Pareto-front where increase (decrease) in one objective is very large compared to decrease (or increase) in other objective.

L_2-metric: This is a straight-forward method to select one solution out of many non-dominated solutions without requiring any information from user. Firstly, each objective is normalized between [0.0, 1.0]. Then an *'ideal point'* is constructed, which is origin in case of normalized space, and taken as the eference point. Euclidean distance (L_2) of each point in non-dominated set is calculated from the reference point and the solution with smallest euclidean distance is finally selected.

Table 2: Parameter Setting for Evolutionary Algorithms

General Parameters:
Population size 40
Generations 80
Runs 11

Other NSGA-II Parameters:
Crossover probabilityi 0.9
Mutation probability 0.5
Crossover Index 10
Mutation Index 20

Other MOPSO Parameters:
Turbulence Factor 0.25
pBest Archive Size 3
Archive Size 200

6 Experiments

In this section a series of simulations are performed on various solid models (ranging from simple geometries to complex ones) to find the optimal build orientations and trade-off fronts for *Ra* and T. A total of 16 solid models are considered in this study: Pyramid, Bi-Pyramid, Cuboid, Cuboidal-Pyramid, Prism, Cylinder, Bracket, Pentagon-Bar, Sharp, Connector, Disc, Fin, Pie, Key, Diamond and Plier. These objects serve as a good representative set with various features.

Both NSGA-II and MOPSO are applied for optimization and performance of these optimizers are compared based on hypervolume curves and attainment surfaces. A population size of 40 and maximum number of generations 80 are chosen for both the optimizers. For each solid model both MOPSO and NSGA-II are executed for 11 runs. Results from multiple runs of both the optimizers are combined and tested for further improvement by proposed local search. Little or negligible improvement is found after local search, indicating the closeness of solutions to the true Pareto-optimal set. Then, the 1^{st}(0%) attainment surface is computed to provide the best approximation of Pareto-front. Study of shapes and spread of Pareto-fronts along with the orientations corresponding to extreme solutions yields highly useful information and insight into optimization problem. Based on the results for optimal orientations solid models are . This categorization helps in drawing general guidelines for optimal orientations. Important task of Decision making is also carried out by demonstrating application of newly introduced decision making methods. The usefulness of each method is also highlighted.

7 Results and Discussions

Estimation of minimum T orientation for SLS is done by aligning the shortest dimension on object along the build direction. However; in general minimum *Ra* orientation is not intutive. *Ra* computation is done using the surface roughness model mentioned in section 3. This *Ra* model was developed based on statistical design of experiments, i.e. firstly factors affecting the *Ra*, like laser power, layer thickness, hatch spacing, scan speed, and build orientation were considered. Then, SLS prototypes were fabricated and in multiple experiments surface roughness measurement was carried out. The obtained values of surface roughness were used and a response and analysis of variance (ANOVA) was performed to understand the significance of chosen factors. Finally surface roughness expressions for 'up' and 'down' surfaces were derived. Due to two separate expressions of 'up' and 'down' facing surfaces, roughness values differ at build angle α=90°. At this angle roughness is computed by taking the average of the values from two models. Overall surface roughness *Ra* is obtained by summing the weighted surface roughnesses of all facets.

From the above discussions it is clear that prediction of minimum *Ra* orientation is not straightforward. Further, at orientations in which majority of the model's surface area has a build angle (α) in proximity of 90°, *Ra* is expected to shown an erratic behaviour. Also, as the surface roughness expressions are statistically derived, rather than being exact, deviations from predicted values are likely to occur in practical cases.

Based on the simulation results in this study, the objects are categorized into two groups: (a) Solid models for which a distributed set of trade-off solutions is obtained, and (b) Solid models for which there is little variation in *Ra* or T over the entire Pareto-front. For group (a) objects, objectives are evidently conflicting leading to a reasonable range of Pareto-optimal solutions, whereas for group (b) the objectives are almost non-conflicting leading to solutions within a small range. The two groups are discussed next:

Group (a): Following solid objects are placed in this category: BiPyramid, Pyramid, Prism, Pentagon-Bar, Disc, Cylinder, Diamond, Wine-Glass and Bracket. For each of these objects hypervolume curves, 1^{st}(0%) attainment surfaces, orientations corresponding to minimum T and minimum *Ra*, and L_2-metric based decision choice are shown in Figures 8 to 13. From the hypervolume curves, Figures 8(a), 9(a),

10(a), 10(f), 11(a), 11(f), 12(a), 12(f) and 13(a), it is evident that NSGA-II outperforms MOPSO in all cases. NSGA-II reaches a higher and steady hypervolume value in lesser number of generations. In most cases MOPSO shows a faster hypervolume rise in initial few generations but fails to match with NSGA-II performance. Such a behavior of MOPSO indicates a pre-mature convergence. According to the authors, such problem arises due to absence of potential global guides and discontinuous function landscapes. However; from the attainment surfaces it can be seen that, MOPSO and NSGA-II have similar convergence and spread (with NSGA-II doing slightly better). The application of two optimizers validates the procedure and builds our confidence in trade-off fronts obtained. On the tarde-off fronts for these solid models, local search (as described in section 4.3) was conducted and practically no improvement was found. Thus, it can be concluded that trade-off solutions found are close to true Pareto-optimal solutions.

For Bipyramid, the minimum T orientation, Figure 8(e), is achieved such that the object almost lies on one of the faces. In this configuration the minimum height along Z-axis (build direction) is obtained. Since the faces of Bipyrism have equal areas, the orientation which minimizes the surface roughness is the one in which the sum of all surface roughnesses is minimized. From the *Ra* model described earlier (Figure 2), roughness for a face is minimum when α is close to zero whether 'up' facing or 'down' facing. With Bipyramid geometry it is impossible to achieve an orientation where all (or a majority) of surfaces have 0° build angle. In such situation a 'best' compromise which minimizes the sum of surface roughnesses is acheived when Bipyramid is slightly tilted from the vertical with majority of surfaces 'up' facing and one face close to being vertical, as shown in Figure 8(f). The L_2-metric decision orientation lies in between the minimum T and *Ra* orientations and is a 'knee' point on the attainment surface. 'Reference Point Method' and 'Marginal Utility' decision schemes are shown in Figures 8(c) and 8(d), respectively. For 'Reference Point Method' three solutions are obtained correspoding to three reference points. The 'Marginal Utility Method' finds a 'knee' solution. From the decision choices obtained for three methods it turns out that 'L_2-metric method' and 'Marginal Utility' method favor to discover a knee solution on the Pareto-front and do not depend upon any user information. 'Aspiration Method' is more flexible in finding solutions which resemble user's preference. However; according to this method solution found, corresponding to a chosen reference point, depends on the shape and spread of the Pareto-front.

For Pyramid, the minimum T orientation is achieved with Pyramid lying horizontally flat on one of its faces, Figure 9(e). This orientation leads to minimum length along Z-axis. In minimum *Ra* orientation, Figure 9(f), the Pyramid axis is slightly titled from the vertical and 3 out of 5 surfaces are 'up' facing, with one of the faces being vertical. The L_2-metric decision again corresponds to 'knee' point and has an orientation close to minimum T orientation. The similarity in nature of extreme solutions obtained for Bipyramid and Pyramid is obvious based on geometrical similarity. The decision choices obtained for Pyramid are shown in Figures 9(b), 9(c) and 9(d). The solutions obtained on the Pareto-front are similar to those obtained for Bipyramid, which can accounted for similarities in 'Bypyramid' and 'Pyramid', and their Pareto-fronts. For remaining solid models only L_2-metric decision choices are shown.

For Prism, in the minimum T orientation, Figure 10(c), the object lies flat on one of the larger faces. In minimum *Ra* orientation, Figure 10(d), 4 out of 5 surfaces are either 'up' facing or vertical. In this orientation Prism assumes an inclined orientation with respect to the horizontal such that one of the larger faces is also vertical. Decision choice based on L_2-metric is found on the 'knee' and has an orientation close to minimum T orientation.

An important observation can be made from the minimum T and *Ra* orientations found for the objects discussed so far. Firstly, in minimum T (or maximum *Ra*) orientations, each object has a surface on which it rests horizontally flat to reduce the length along Z-axis. For a flat surface the build angle $\alpha=90^\circ$. From the surface roughness models it is clear that for an 'up' or 'down' facing surface maximum roughness occurs at $\alpha=90^\circ$. Hence, it is no surprise that a solution which minimizes T has a maximum *Ra*. Similar analysis can be carried out for minimum *Ra* orientations. For all the minimum *Ra* orientations it is found that there exists at least one face with larger surface area which is almost vertical (i.e. with $\alpha=0^\circ$). Again referring to the models, roughness is minimum for a face when $\alpha=0^\circ$. Hence, it is no surprise to have a vertical face (one with the maximum surface area) leading to minimum roughness for the face. Moreover,

roughness models also suggest that for smaller values of α, 'up' faces have lower surface roughness as compared to 'down' faces, this fact is consistent with the observation that in minimum *Ra* orientations majority of surfaces are 'up' facing. The arguments presented in this discussion can be referred to explain the solutions obtained for remaining solid models.

For Pentagon-Bar minimum *T* orientation, Figure 10(h), occurs with the object lying flat on one its faces and minimum height is acheived alng Z-axis. In minimum *Ra* orientation, Figure 10(h), all the large faces of the bar are vertical causing the build angle α=0°. The $L-2$ metric decision choice is again a 'knee' solution and slighlty titled from minimum *T* orientation.

For Disc minimum *T* orientation, 11(c), occurs with Disc lying horizontally flat, allowing minimum dimension (disc height) along Z-axis. The minimum *Ra* orientation, 10(d), occurs with flat surfaces of disc vertical. In vertical position (α=0°) flat surfaces have least roughness based on the models. Large combined area of flat surfaces compared to curved surface area assigns more weight lower roughness and thus *Ra* is minimized. L_2 metric decision choice is not exactly horizontal (like minimum *T* orientation) and has (θ_x, θ_y)=$(89.72°, 180°)$ and corresponds to a 'knee' solution.

To validate our line of arguments, Cylinder is considered next. The length of the Cylinder is chosen to be larger than its diameter (unlike Disc). The minimum *T* orientation occurs with Cylinder lying horizontal and flat faces vertical, Figure 11(h). In minimum *Ra* orientation, Figure 11(i), Cylinder stands tall vertically on one of the flat surfaces. This configuration is justified because larger curved surface area has lower surface roughness in vertical position with α=0°, and as *Ra* is weighted with surface area, minimum value is acheived in this orientation. The L_2-metric decision choice resembles closely to minimum *T* orientation and corresponds to a solution on 'knee' of the Pareto-front.

Next object considered is Diamond. The minimum *T* orientation, Figure 12(c), is self explainatory. The minimum *Ra* orientation, Figure 12(d), occurs with axis of Diamond titled with respect to vertical and flat top facing 'down' and major portion of the curved surface area facing 'up'. For Diamond the curved surface area is much larger than the flat top area, and from previous discussions we already have noted that 'down' facing leads to higher roughness compared to 'up' facing (upto certain α values). Thus, in minimum *Ra* orientation larger part of surface area is 'up' facing. On the Pareto-front,L_2-metric based decision choice is lies very close to minimum *T* solution and also has similar 3-D orientation.

Second last object belonging to this group is Wine-Glass. The front view indicates an interesting orientation taken up for minimizing *T*, Figure 12(h). In minimum *Ra* orientation, 12(h), the object axis is tilted with the vertical, and majority of curved surface takes an 'up' facing orientation. L_2-metric based decision choice is again a 'knee' solution with object axis almost horizontal.

Final object in this category is Bracket. The minimum *T* orientation, Figure 13(c), assumes horizontally resting position with convex surface projecting upwards. An interesting analysis leads to better understanding that why convex surface (and not concave surface) faces 'up' in the minimum *T* orientation. The reason found for this is consistent with the arguments presented in the paper so far and stated as follows: Firstly, the convex side of Bracket has a larger area compared to concave side. We also know that upto certain α values 'up' facing surface has lower roughness values compared to 'down' facing, and orientations in which majority surface area is up facing is preferred for miniming *Ra*. For the two orientations - one with convex surface 'up' and another with concave surface 'up', build times are same for both but *Ra* is larger for latter, rendering it to be dominated by the prior and getting eliminated from the Pareto-set. For minimizing *Ra*, an orientation in which α=0° for curved surfaces (majority area) is achieved, which is consistent with the fact that α=0° leads to lowest roughness for a face. The L_2-metric decision point is close to minimum *Ra* solution and also lies on 'knee' of the Pareto-front.

Group (b): This group comprises of solid objects for which optimal solutions are found to lie in a small distribution. Solid models in this group are Cuboid, Cuboidal-Pyramid, Connector, Fin, Key, Pie, Sharp and Wire-Plier. For all these objects it is found that the spread of solutions in one of the two objectives is practically negligible. For Cuboid, Figure 14, it can be observed that minimum *T*, minimum *Ra* and decision choice solutions have similar horizontal orientation. From the attainment surface curves it can be clearly seen that spread of solutions along *T* is negligible. Thus, for all these solutions build

time estimate is almost equal, while there is a small variation in *Ra*. The small variation in *Ra* can be explained by again referring to quadratic surface roughness models. For a vertical surface which is neither 'up' or 'down', roughness is computed by averaging the roughnesses of the face by treating it both as 'up' or down 'facing', and since these two values in general are unequal, a discontinuity in roughness is introduced. Additionally, due to numerical and round-off errors in rotation models, *Ra* for two seemingly alike orientations, for e.g. (0°, 0°) and (0°, 180°), may be different slightly different. Thus, in reality small variation in *Ra* is unimportant from a practical view-point, more so when the orientations corresponding to solutions in the small distribution are seemingly alike. The minimum T solution for Cuboid is justified as minimum dimension is along Z-axis. This orientation also has 4 surfaces (majority of the surface area) almost vertical ($\alpha = 0^\circ$) leading to minimum *Ra*.

Cuboidal-Pyramid, Figure 15(a), optimal orientation is similar to optimal orientation of Cuboid. Geometrical similarity between the two objects in "cuboid" part is an obvious reason. Moreover in lying flat orientation, the majority of the surface area on Cuboidal-Pyramid has build angle $\alpha = 0^\circ$ (including two side faces on the Pyramid head), causing overall minimum *Ra*.

Next, for the Pie shape flat orientation, Figure 15(c), is the optimal orientation. From attainment surface curve, 15(b), it can be seen that all solutions have approximately same T values and distribution along *Ra* is also small. Minimum build time in the shown optimal orientation is self-evident. In this minimum *Ra* orientation $\alpha = 0^\circ$ for the side strip. It should be noted that side strip in Pie does not corresponds to majority surface area, and majority surface areas (flat faces) lie horizontal with $\alpha = 90^\circ$. This behaviour is found contrary to earlier observations where in minimum *Ra* orientations majority surface area possessed a build angle $\alpha = 0^\circ$. To understand this behaviour other orientations are shown in which majority surface areas have $\alpha = 0^\circ$, Figures 15(d) and 15(e). It is found that T and *Ra* values are larger for these orientations. This can be explained based on the fact that though the flat vertical surfaces have $\alpha = 0^\circ$, remaning part areas on the strip are found to have large α values, and thus increasing *Ra*. The lowering of *Ra* due to vertical flat surfaces is defiled by increase in *Ra* due to strip area in this configuration.

For remaining objects in this group, single optimal orientation corresponding to minimum T and *Ra* values is shown. In case of Fin, Figure 16(a), the shown orientation has majority surface area with $\alpha = 0^\circ$ (minimizing *Ra*) and minimum vertical thickness (minimizing T). The majority surface area on the Fin comprises of a hollow feature and protruding fin-plates on the surface.

Arguments presented in Pie and Fin examples can be utilized to explain optimal orientations for Key, Figure 16(b). Key comprises of multiple grooves (which increase the area) and a hollow in the key head. In the shown orientation $\alpha = 0^\circ$ for the curved part on Key head and the grooved area at the Key end. Occurence of minimum T in this orientation is straight-forward. Minimum *Ra* is explained on the fact that $\alpha = 0^\circ$ for the groove part, hollow and the curved side area on the Key head. In any other orientation *Ra* increases because of the larger α values associated with the curved Key head (similar to the Pie).

Optimal orientations corresponding to minimum T and *Ra* for Plier, Connector and Sharp are shown in Figures 16(c), 17(a) and 17(b). The flat lying positions of these solid models are similar to optimal orientations for other models in the group and can be explained based on the preceeding discussions. For e.g., minimum T for Sharp is evident. The minimum *Ra* can be attributed to $\alpha = 0^\circ$ for side area, and the fact that in any other orientation the faces on triangular end of Sharp will have a greater α leading to increase in *Ra*. To support this argument we consider a thin Sharp for which side area is almost negligible. For such a Sharp contribution to *Ra* due to side area will be negligible, irrespective of α, as the side area is negligible. Thus, it is expected that for this thin Sharp minimum *Ra* orientation should occur with majority surface area vertical (aligned along Z-axis). This does happen as shown in Figure 17(c), further in minimum *Ra* orientation it is found that the pointed end faces down. The facing down is explained on the fact that for larger α values (close to 45°) the 'down' facing surface has lower roughness compared to 'up' facing. The minimum T orientation for thin Sharp is obviously same as shown in Figure 17(b) leading the minimum dimension to align with Z-axis.

The examples presented here provide an important information - a path to approximately guess the optimal orientation without actually carrying out optimization. A designer can analyze the features on

any new object for which build orientation is to be decided, and relate them to already pre-optimal studies carried out for other objects to come up with a guiding principles. This is analogous to the principle of *Innovization* - discovery of Innovative design principles through Optimization []. For several routine purposes an exhaustive optimization study to discover most appropriate build orientations is impractical. In such cases pre-existing guidelines, to arrive at optimal build orientations, derived from previosly considered optimization studies will be highly useful.

8 Conclusions

This paper presents a novel and systematic approach to address the tasks of finding optimal build orientations in SLS process, approximating true (or close to) Pareto-optimal solutions, and addressing the issue of decision. The entire procedure is integrated leading to the development of *MORPE* - Multi-objective Rapid Prototyping Engine. Two popular optimizers, NSGA-II and MOPSO, are employed to discover trade-off fronts. Although, overall NSGA-II outperforms MOPSO, similarities in convergence and spread of trade-off fronts found by both the optimizers indicates the closeness of obtained solutions to global Pareto-front. Local search emplouyed to fine tune the obtained solutions practically showed no improvement, assuring that solutions found by the optimizers are pretty good estimate for true Pareto-solutions. Several sample objects were considered for bi-objective optimization and post-optimal analysis.Based on the nature of the optimal solutions, objects were divided into two groups. For the first group a reasonable spread amongst the trade-off solutions is found. The second group objects are found to have a single optimal orientation which minimizes both T and Ra. A closer analysis of obtained solutions in consideration with their geometric features and Ra models unfolds common key-characteristics among the optimal orientations. Such discovery is validated through multiple examples and finally a set of guidelines can be formed for a designer aiding him to discover favorable orientations without actually carrying out optimization.

In future, authors are interested in exploring classification methods that can be utilized to form classes or groups of solid-models based on their physical features. Several already existing feature extraction algorithms can be employed for identifying key features. The groups can be further sub-divided into several sub-groups or sub-classes based on their optimal orientations, nature and shape of Pareto-fronts. This pre-classification can be employed for training the learning algorithms. Whenever a new solid model is considered the trained algorithms can be used for predicting the optimal orientation. The predicted optimal orientation can be verified for its accuracy and in case of inconsistency a feed-back based mechanism can be looped back for self-rectification. Finally, a *'Smart System'* can be evolved which can precisely predict the optimal orientations involving least computation.

9 Acknowledgements

First and second authors greatly appreciate the input of Dr. N.V. Reddy and Dr. P.M. Pandey in introducing the problem and guiding all throughout.

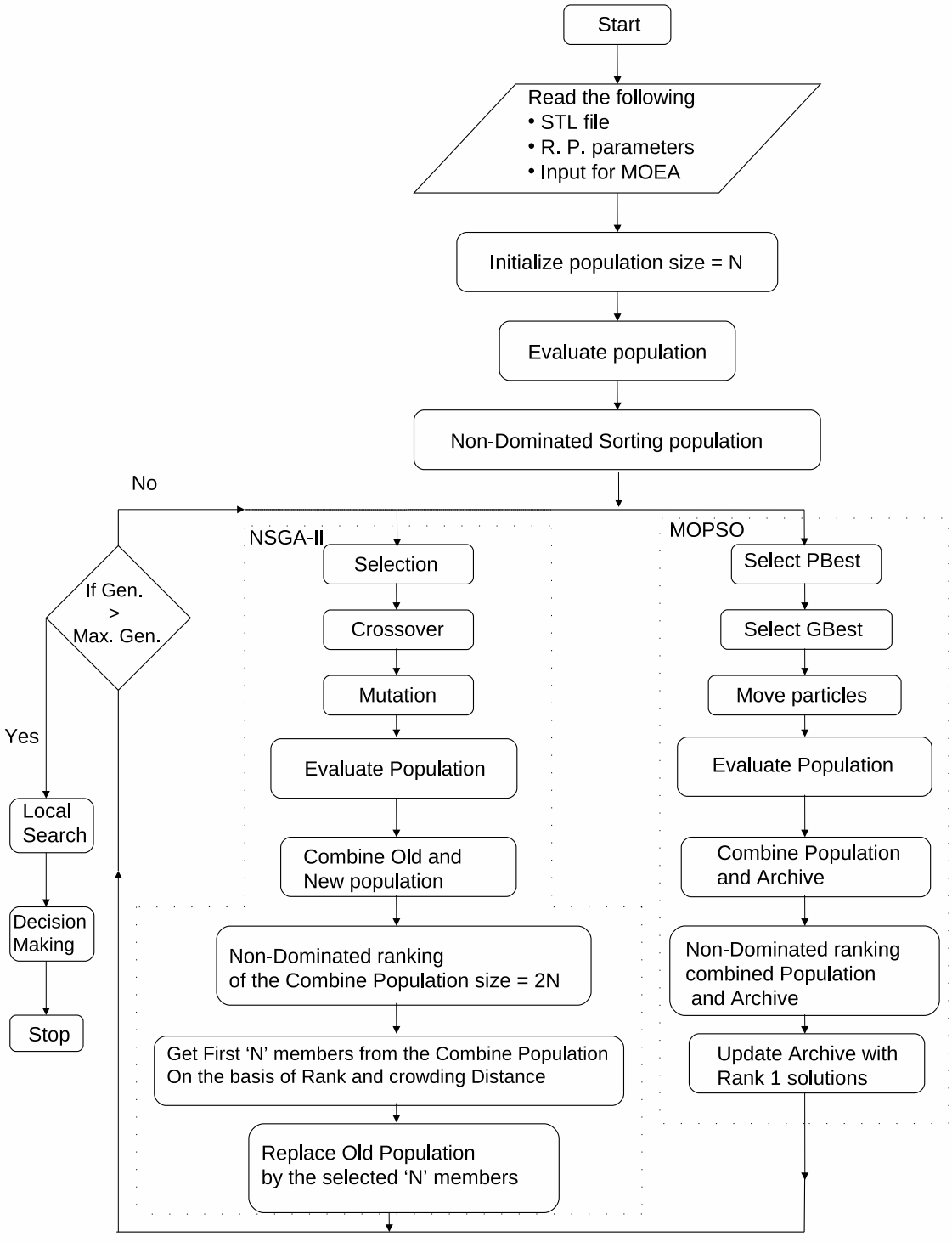

Figure 4: Flowchart suggesting the working of developed engine

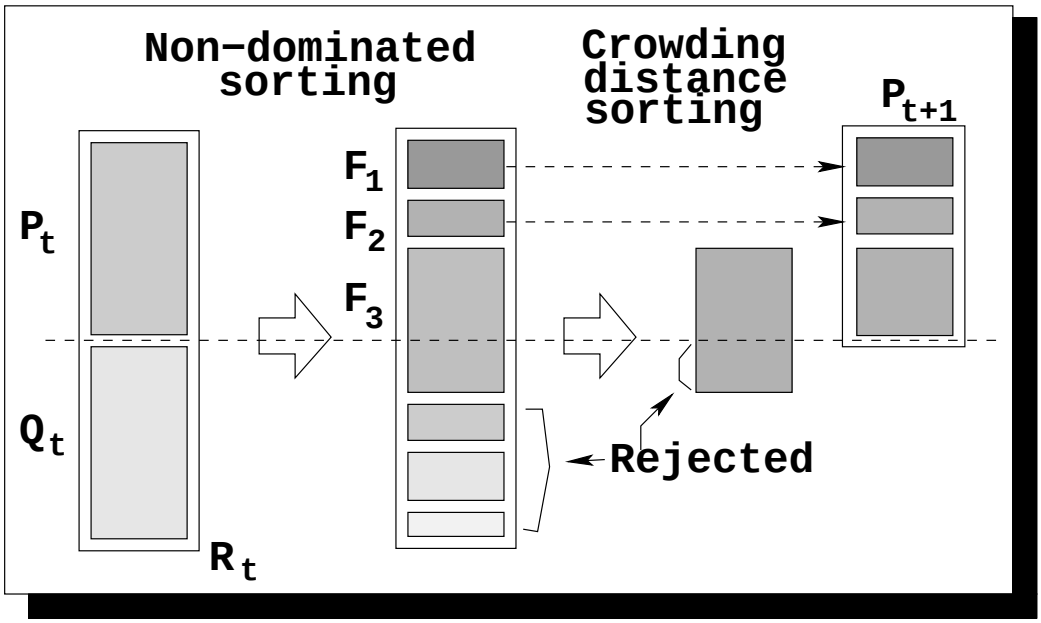

Figure 5: NSGA-II description showing ’elitism’ and ’diversity preservation’.

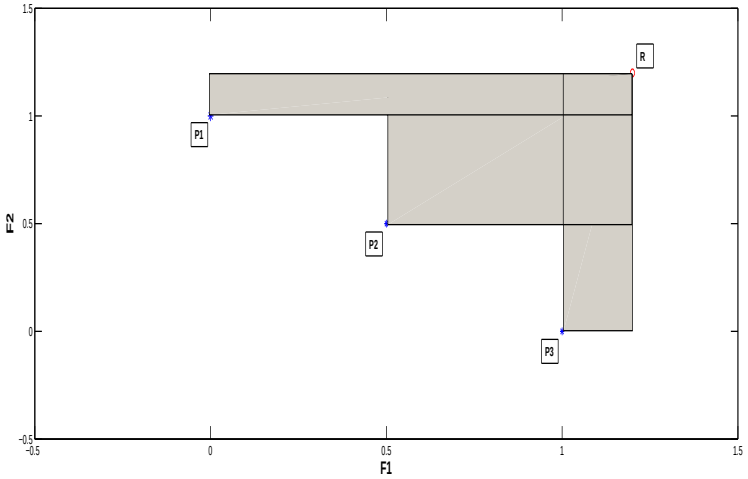

(a) *'Hypervolume Computation'*- P_1,P_2 and P_3 are three non-dominated solutions, and R is chosen reference point. Total area enclosed by the hypercubes (in this case rectangles) formed by non-dominated points and reference point equals the hypervolume.

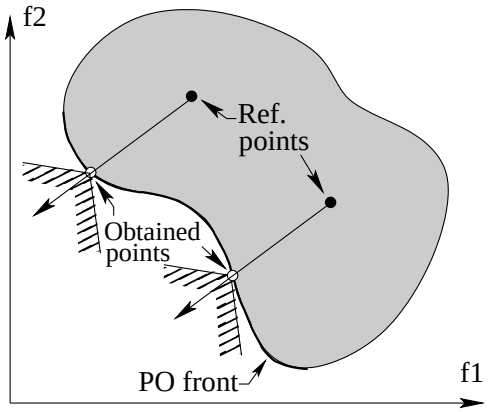

(b) Achievement Scalarization based *Local Search*

Figure 6: Various edge detection algorithms

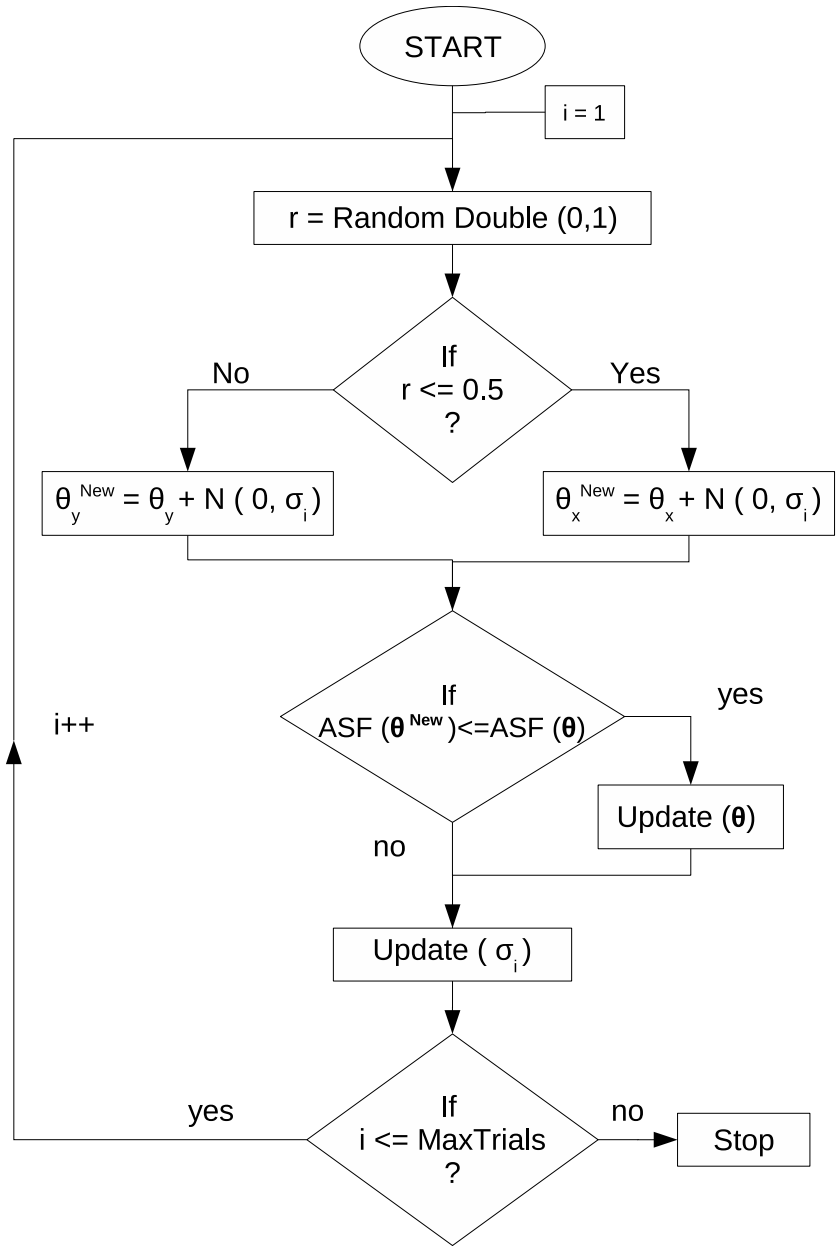

Figure 7: Hill Climbing Local Search

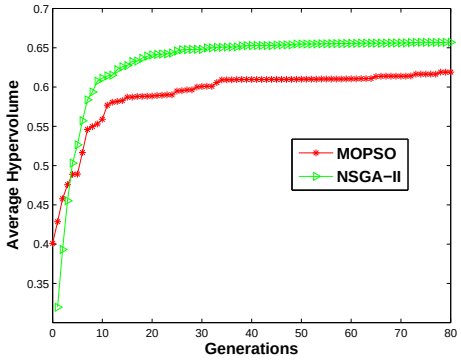

(a) Average Hypervolume Curves for Bipyramid with reference point (11.5, 11.0)

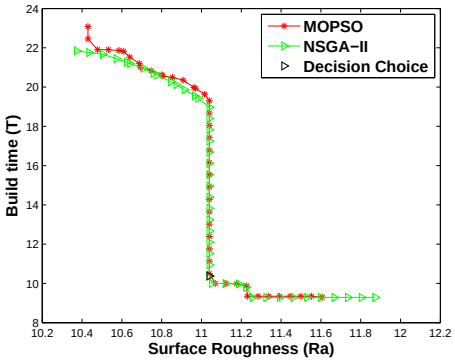

(b) 1^{st} Attainment Surfaces for NSGA-II and MOPSO and L_2-metric Decision Choice for Bipyramid

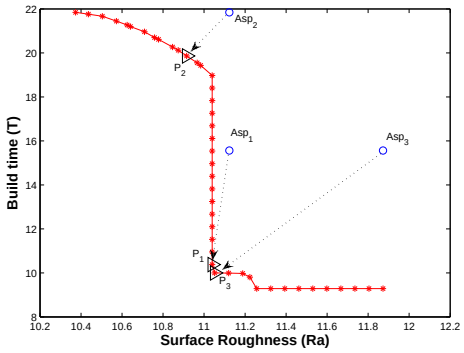

(c) Reference Point method for Bipyramid

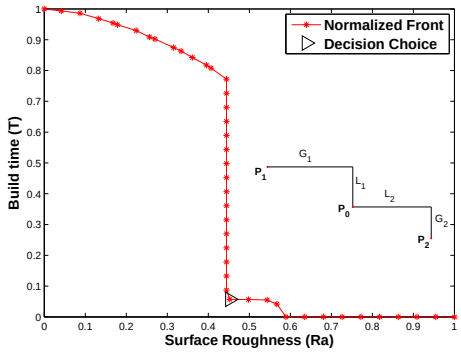

(d) Marginal Utility method for Bipyramid

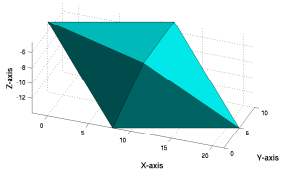

(e) Min. time orientation (θ_x,θ_y)= (0.0°, 111.81°), (*Ra*, *T*)= (11.87, 9.29)

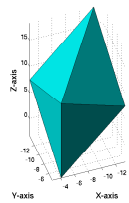

(f) Min. Ra orientation (θ_x,θ_y)= (158.2°, 159.63°), (*Ra*, *T*)= (10.37, 21.76)

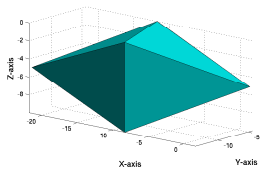

(g) L_2-metric Decision Choice orientation for (θ_x,θ_y)= (159.94°, 90.01°), (*Ra*, *T*)= (11.04, 10.00)

Figure 8:

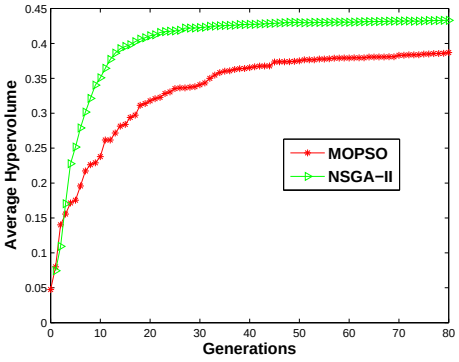

(a) Average Hypervolume Curves for Pyramid with reference point (10.0, 11.0)

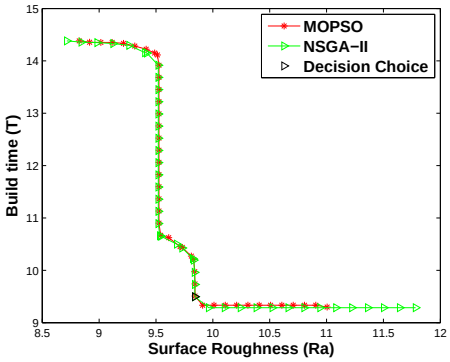

(b) 1^{st} Attainment Surfaces for NSGA-II and MOPSO and L_2-metric Decision Choice for Pyramid

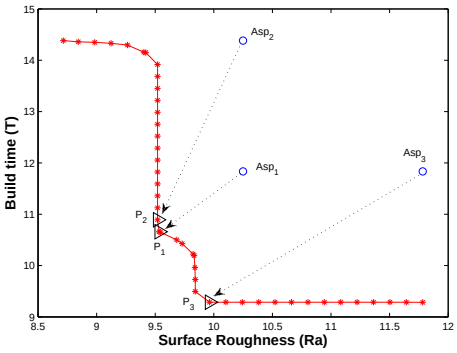

(c) Reference Point method for Pyramid

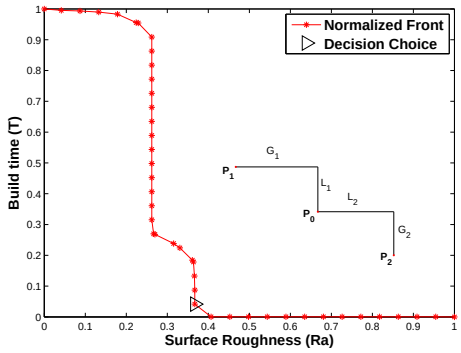

(d) Marginal Utility method for Pyramid

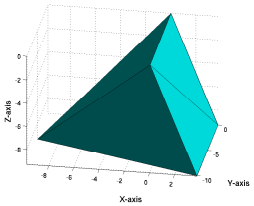

(e) Min. time orientation (θ_x,θ_y)= (180.0°, 68.19°), (*Ra*, *T*)= (11.77, 9.29)

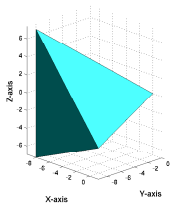

(f) Min. Ra orientation (θ_x,θ_y)= (158.2°, 159.64°), (*Ra*, *T*)= (8.72, 14.36)

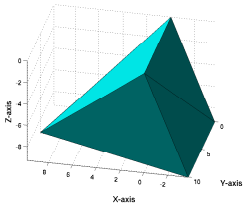

(g) L_2-metric Decision Choice orientation for (θ_x,θ_y)= (0.0°, 111.5326°), (*Ra*, *T*)= (9.84, 9.30)

Figure 9:

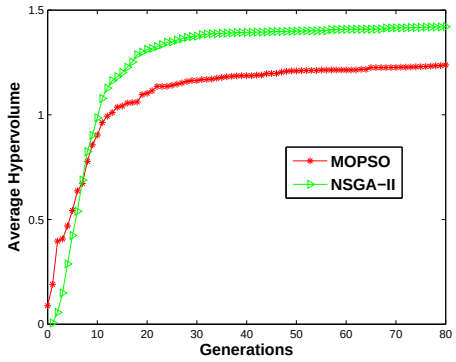

(a) Average Hypervolume Curves for Prism with reference point (10.0, 12.0)

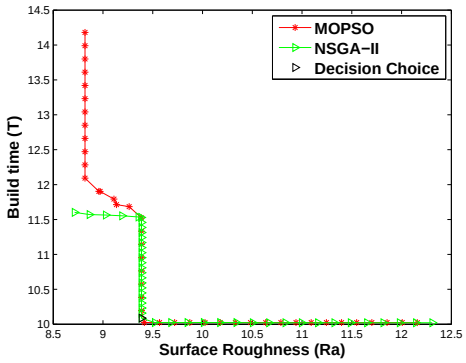

(b) 1^{st} Attainment Surfaces for NSGA-II and MOPSO and L_2-metric Decision Choice for Prism

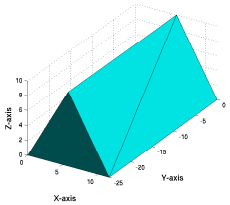

(c) Min. time orientation (θ_x,θ_y)= (90.0°, 0.0°), (*Ra*, *T*)= (12.29, 10.02)

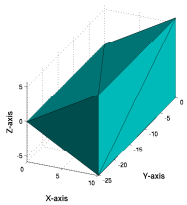

(d) Min. Ra orientation (θ_x,θ_y)= (89.99°, 29.99°), (*Ra*, *T*)= (8.71, 11.57)

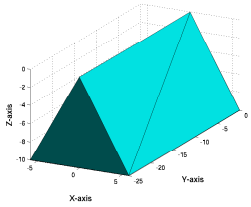

(e) L_2-metric Decision Choice orientation for (θ_x,θ_y)= (90.09°, 119.83°), (*Ra*, *T*)= (9.40, 10.06)

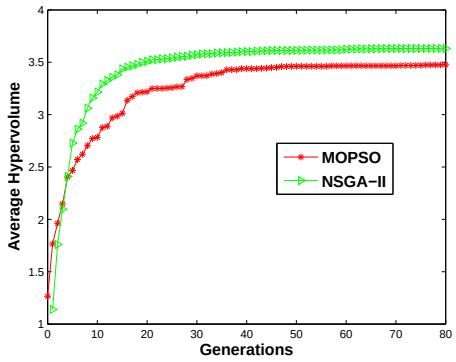

(f) Average Hypervolume Curves for PentagonBar with reference point (12.5, 17.0)

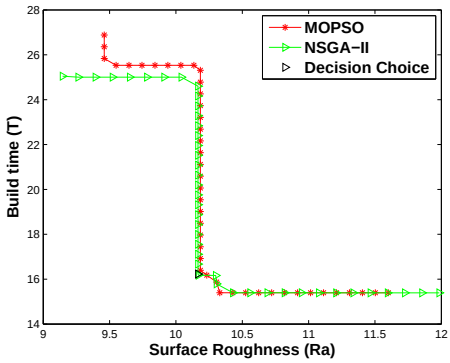

(g) 1^{st} Attainment Surfaces for NSGA-II and MOPSO and L_2-metric Decision Choice for Pentagon-Bar

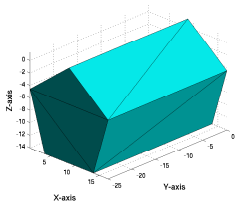

(h) Min. time orientation (θ_x,θ_y)= (90.0°, 81.45°), (*Ra*, *T*)= (11.89, 15.38)

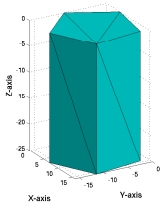

(i) Min. Ra orientation (θ_x,θ_y)= (179.99°, 0.02°), (*Ra*, *T*)= (9.15, 25.0)

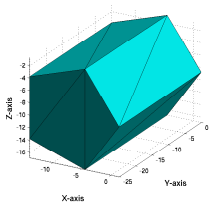

(j) L_2-metric Decision Choice orientation for (θ_x,θ_y)= (90.02°, 171.5°), (*Ra*, *T*)= (10.17, 16.19)

Figure 10:

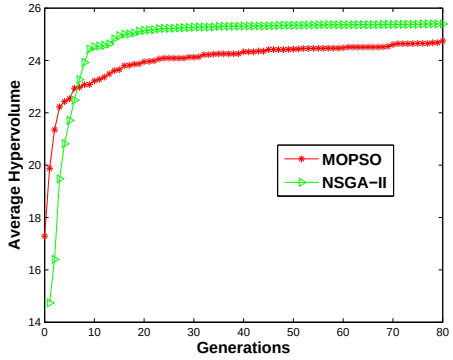

(a) Average Hypervolume Curves for Disc with reference point (14.0, 13.5)

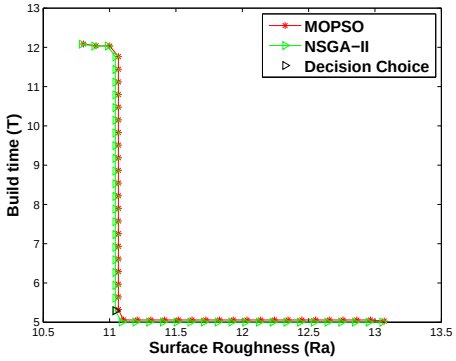

(b) 1st Attainment Surfaces for NSGA-II and MOPSO and L_2-metric Decision Choice for Disc

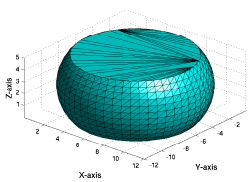

(c) Min. time orientation (θ_x,θ_y)= (90.0°, 0.0°), (*Ra*, *T*)= (12.13, 5.0)

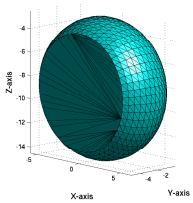

(d) Min. Ra orientation (θ_x,θ_y)= (180.0°, 43.33°), (*Ra*, *T*)= (10.85, 12.05)

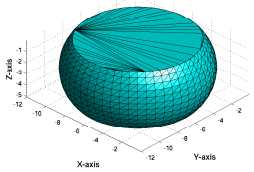

(e) L_2-metric Decision Choice orientation for (θ_x,θ_y)= (89.72°, 180.0°), (*Ra*, *T*)= (11.064, 5.048)

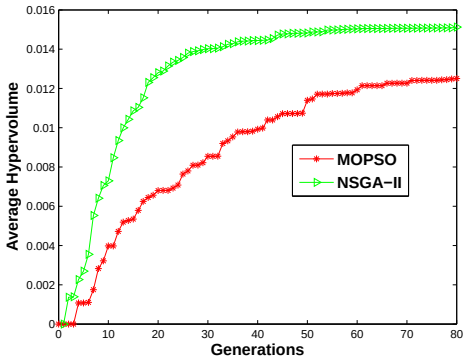

(f) Average Hypervolume Curves for Cylinder with reference point (11.0, 10.0)

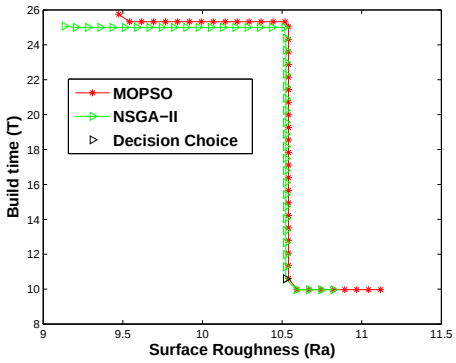

(g) 1st Attainment Surfaces for NSGA-II and MOPSO and L_2-metric Decision Choice for Cylinder

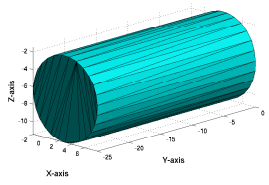

(h) Min. time orientation (θ_x,θ_y)= (90.0°, 110.09°), (*Ra*, *T*)= (10.73, 9.99)

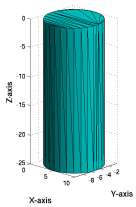

(i) Min. Ra orientation (θ_x,θ_y)= (179.98°, 0.0°), (*Ra*, *T*)= (9.13, 25.0)

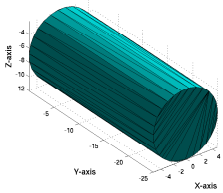

(j) L_2-metric Decision Choice orientation for (θ_x,θ_y)= (90.0°, 136.65°), (*Ra*, *T*)= (10.52, 9.97)

Figure 11:

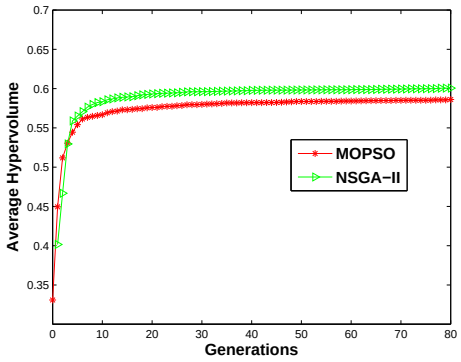

(a) Average Hypervolume Curves for Diamond with reference point (11.5, 12.0)

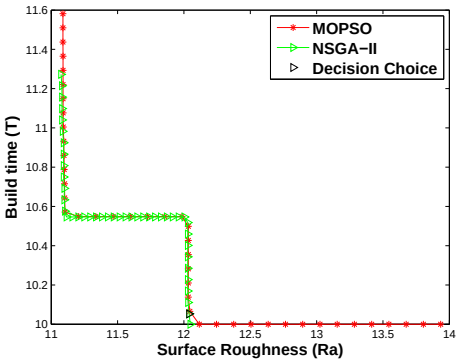

(b) 1st Attainment Surfaces for NSGA-II and MOPSO and L_2-metric Decision Choice for Diamond

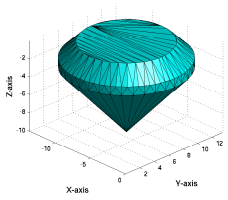

(c) Min. time orientation (θ_x,θ_y)= (0.0°, 180.0°), (*Ra*, *T*)= (12.04, 10.0)

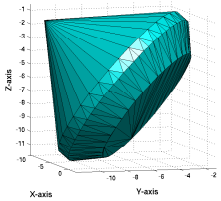

(d) Min. Ra orientation (θ_x,θ_y)= (138.3°, 145.24°), (*Ra*, *T*)= (11.07, 11.26)

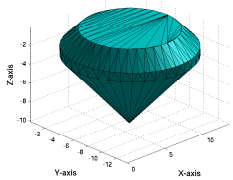

(e) L_2-metric Decision Choice orientation for (θ_x,θ_y)= (180.0°, 0.6°), (*Ra*, *T*)= (12.04, 10.05)

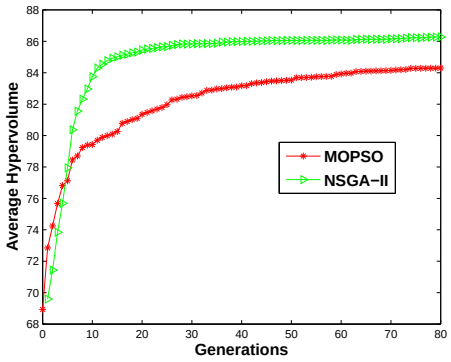

(f) Average Hypervolume Curves for WineGlass with reference point (13.0, 125.0)

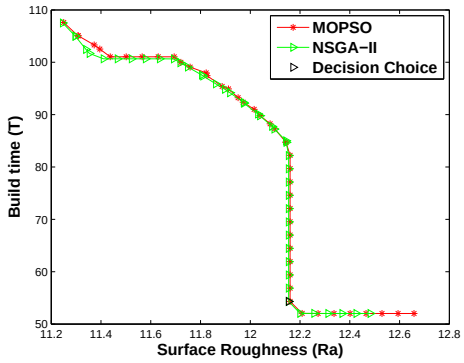

(g) 1st Attainment Surfaces for NSGA-II and MOPSO and L_2-metric Decision Choice for Wine-Glass

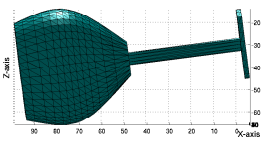

(h) Min. time orientation (θ_x,θ_y)= (7.34°, 180.0°), (*Ra*, *T*)= (12.48, 52.0)

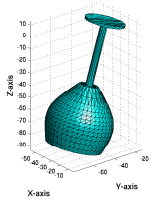

(i) Min. Ra orientation (θ_x,θ_y)= (107.75°, 180.0°), (*Ra*, *T*)= (11.25, 107.27)

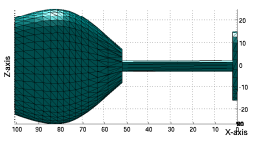

(j) L_2-metric Decision Choice orientation for (θ_x,θ_y)= (0.01°, 45.94°), (*Ra*, *T*)= (12.15, 52.09)

Figure 12:

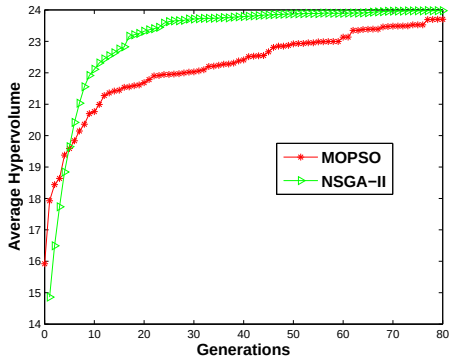

(a) Average Hypervolume Curves for Bracket with reference point (12.0, 40.0)

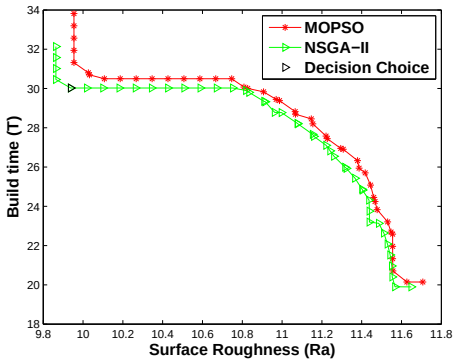

(b) 1^{st} Attainment Surfaces for NSGA-II and MOPSO and L_2-metric Decision Choice for Bracket

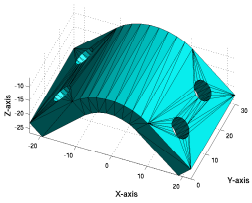

(c) Min. time orientation (θ_x,θ_y)= (0.0°, 135.0°), (*Ra*, *T*)= (11.64, 19.9)

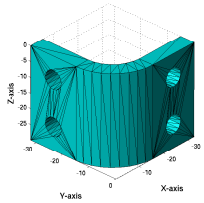

(d) Min. Ra orientation (θ_x,θ_y)= (90.04°, 180.0°), (*Ra*, *T*)= (9.86, 30.03)

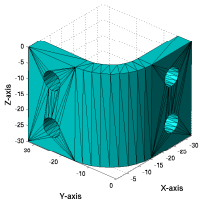

(e) L_2-metric Decision Choice orientation for (θ_x,θ_y)= (90.36°, 179.98°), (*Ra*, *T*)= (9.89, 30.21)

Figure 13:

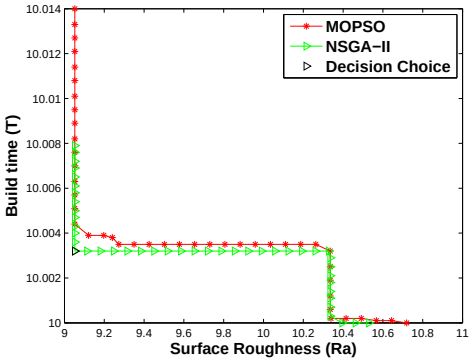

(a) 1^{st} Attainment Surfaces for NSGA-II and MOPSO and L_2-metric Decision Choice for Cuboid

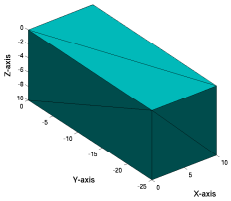

(b) Min. time orientation (θ_x,θ_y)= (90.0°, 90.0°), (*Ra*, *T*)= (10.52, 10.0)

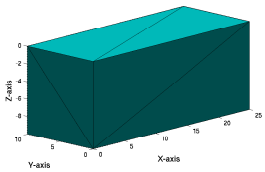

(c) Min. Ra orientation (θ_x,θ_y)= (0.0°, 89.98°), (*Ra*, *T*)= (9.05, 10.0)

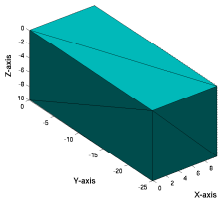

(d) L_2-metric Decision Choice orientation for (θ_x,θ_y)= (90.25°, 90.02°), (*Ra*, *T*)= (9.24, 10.00)

Figure 14:

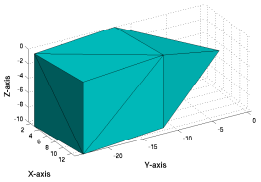

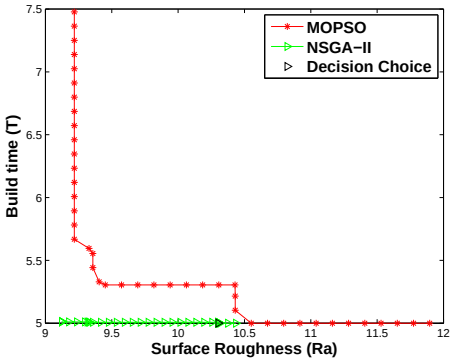

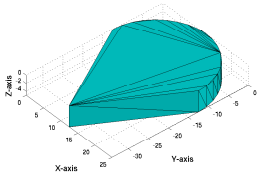

(a) Optimal orientation for Cuboidal-Pyramid (θ_x,θ_y)= (83.33.0°, 90.0°), (Ra, T)= (10.6, 10.0)

(b) 1^{st} Attainment Surfaces for NSGA-II and MOPSO and L_2-metric Decision Choice for Pie

(c) Optimal orientation for Pie (θ_x,θ_y)= (180.0°, 0.0°), (Ra, T)= (10.43, 5.0)

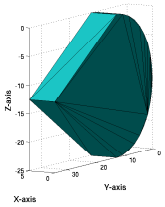

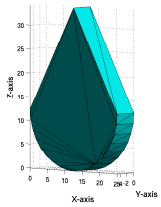

(d) Orientation with (θ_x,θ_y)= (0°, 90°), (Ra, T)= (11.16, 25.0)

(e) Orientation with (θ_x,θ_y)= (90°, 0°), (Ra, T)= (11.85, 34.1)

Figure 15:

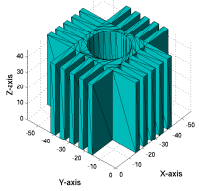

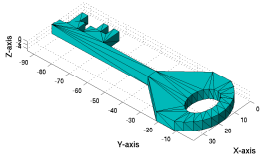

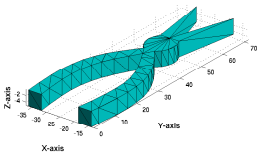

(a) Optimal orientation for Fin (θ_x,θ_y)= (180.0°, 180.0°), (Ra, T)= (9.27, 45.0)

(b) Optimal orientation for Key, (θ_x,θ_y)= (180.0°, 0.0°), (Ra, T)= (9.56, 5.0)

(c) Optimal orientation for Plier (θ_x,θ_y)= (0°, 180.0°), (Ra, T)= (9.29, 5.0)

Figure 16:

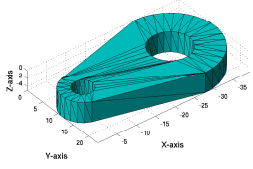

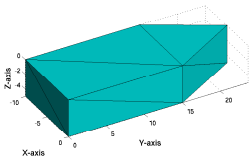

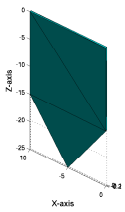

(a) Optimal orientation for Connector (θ_x,θ_y)= (0.0°, 180.0°), (Ra, T)= (9.8, 5.0)

(b) Optimal orientation for Sharp, (θ_x,θ_y)= (0.0°, 180.0°), (Ra, T)= (10.53, 5.0)

(c) Minimum Ra orientation for thin Sharp, (θ_x,θ_y)= (90.0°, 180.0°), (Ra, T)= (10.029, 25.0)

Figure 17:

References

[1] Daekeon Ahn, Hochan Kim, and Seokhee Lee. Fabrication direction optimization to minimize post-machining in layered manufacturing. *International Journal of Machine Tools and Manufacture*, 47(3-4):593 – 606, 2007.

[2] Hong-Seok Byun and Kwan H. Lee. Determination of the optimal build direction in layered manufacturing using a genetic algorithm. *Internation Journal of Production Research*, 43(13):2709–2724, 2005.

[3] Hong-Seok Byun and Kwan H. Lee. Determination of the optimal build direction for different rapid prototyping processes using multi-criterion decision making. *Robotics and Computer-Integrated Manufacturing*, 22(1):69 – 80, 2006.

[4] V. Canellidis, J. Giannatsis, and V. Dedoussis. Genetic-algorithm-based multi-objective optimization of the build orientation in stereolithography. *The International Journal of Advanced Manufacturing Technology*, 2009.

[5] W. Cheng, J. Y. H. Fuh, , A. Y. C. Nee, Y. S. Wong, H. T. Loh, and T. Miyazawa. Multi-objective optimization of part-building orientation in stereolithography. *Rapid Prototyping Journal*, 1:22–33, 1995.

[6] C. K. Chua, K. F. Leong, and C. S. Lim. *Rapid Prototyping: Principal and Applications 2nd Edition*. Word Scientific Publishing Co. Ltd., 2003.

[7] K. Deb. *Multi-objective Optimization Using Evolutionary Algorithms*. John Wiley and Sons, Dordrecht, 2001.

[8] K. Deb, S. Agarwal, and T. Meyarvian. A fast and elitist multi-objective genetic algorithm: Nsga-ii. *IEEE Transactions on Evolutionary Computation*, 6(2):182–197, 2002.

[9] D.T. Dimov D.T. Pham and R.S. Gault. Part orientation in stereolithography. *International Journal of Advanced Manufacturing Technology*, 15:674–682, 1999.

[10] D. Frank and G. Fadel. Expert system-based selection of the preferred direction of build for rapid prototyping processes. *Journal of Intelligent Manufacturing*, (6):339–345, 1995.

[11] A. Goyal, A. Sudha, A. Kumar, and P. V. M. Rao. Optimum part orientation for rapid prototyping based on estimated number of adaptive slices. In *Proceedings of International Conference on E-manufacturing*, pages 247–253, 2002.

[12] J. Hong, W. Wang, and Y. Tang. Part building orientation optimization method in stereolithography. *Chinese Journal of Mechanical Engineering (English Edition)*, 19(1):14–18, 2006.

[13] H.C. Kim and S.H. Lee. Reduction of post-processing for stereolithography systems by fabrication-direction optimization. *Computer Aided Design*, 37(7):711–725, 2005.

[14] J. Knowles. A summary-attainment-surface plotting method for visualizing the performance of stochastic multiobjective optimizers. In *IEEE Intelligent Systems Design and Applications (ISDA V)*, pages 552–557, 2005.

[15] J.P. Kruth, M.C. Leu, and T. Nakagawa. Progress in additive manufacturing and rapid prototyping. *Annals of CIRP*, 47(2), 1998.

[16] P.-T. Lan, S.-Y. Chow, L.-L. Chen, and D. Gemmill. Determining fabrication orientations for rapid prototyping with stereolithography apparatus. *Computer Aided Design*, 29:53–62, 1997.

[17] J. A. Leitao, R. Everson, N. Sewell, and M. Jenkins. Multi-objective optimal positioning and packing for layered manufacturing. In *Proceedings of the 3rd International Conference on Advanced Research in Virtual and Rapid Prototyping: Virtual and Rapid Manufacturing Advanced Research Virtual and Rapid Prototyping*, pages 655–660, 2008.

[18] S. H. Masood and W. Rattanawong. A generic part orientation system based on volumetric error in rapid prototyping. *International Journal of Advanced Manufacturing Technology*, 19(3):209–216, 2000.

[19] S. H. Masood, W. Rattanawong, and P. Iovenitti. Part build orientations based on volumetric error in fused deposition modeling. *International Journal of Advanced Manufacturing Technology*, 19:162–168, 2000.

[20] N. Padhye. Comparision of archiving methods in mopso: Empirical study. In *GECCO '09: Proceedings of the 2009 GECCO conference companion on Genetic and evolutionary computation*.

[21] N. Padhye. Topology optimization of compliant mechanism using multi-objective particle swarm optimization. In *GECCO '08: Proceedings of the 2009 GECCO conference companion on Genetic and evolutionary computation*, pages 1831–1834.

[22] N. Padhye, J. Juergen, and S. Mostaghim. Empirical comparison of mopso methods - guide selection and diversity preservation -. In *Proceedings of Congress on Evolutionary Computation (CEC), in press*. IEEE, 2009.

[23] N. Padhye and S. Kalia. Rapid prototyping using evolutionary algorithms: Part 1. In *GECCO '09: Proceedings of the 2009 GECCO conference companion on Genetic and evolutionary computation*, 2009.

[24] N. Padhye and S. Kalia. Rapid prototyping using evolutionary algorithms: Part 2. In *GECCO '09: Proceedings of the 2009 GECCO conference companion on Genetic and evolutionary computation*, pages 2737–2740, 2009.

[25] P. M. Pandey, K. Thrimurthulu, and N. V. Reddy. Optimal part deposition orientation in fdm by using a multicriteria. *International Journal of Production Research*, 42 (19):4069–4089, 2004.

[26] P.M. Pandey, N. Venkata Reddy, and S.G. Dhande. Part deposition orientation studies in layered manufacturing. *Journal of Materials Processing Technology*, 185:125–131, 2007.

[27] S.K. Singhal, Prashant K. Jain, Pulak M. Pandey, and A.K. Nagpal. Optimum part deposition orientation for multiple objectives in sl and sls prototyping. *International Journal of Production Research*, 47 (22):6375–6396, 2009.

[28] K. Thrimurtullu, P.M. Pandey, and N. V. Reddy. Optimum part deposition orientation in fused deposition modeling. *International Journal of Machine Tools and Manufacture*, 4(6):585–594, 2004.

[29] A. P. West, S. P., and D. W. Rosen. A process planning method to improve build performance in stereolithography. *Computer Aided Design*, 33:65–79, 2001.

[30] F. Xu, S.Y. Wong, T.H. Loh, HYJ Fuh, and T Miyazawa. Optimal orientation with variable slicing in stereolithography. *Rapid Prototyping Journal*, 3(3):76–88, 1997.

[31] L. Q. Zhang, D.-H. Xiang, M. Chen, and B.-X. Wang. Optimum design for rp deposition orientation by genetic algorithm. *Nanjing Hangkong Hangtian Daxue Xuebao/Journal of Nanjing University of Aeronautics and Astronautics 37 (SUPPL.)*, pages 134–136, 2005.

[32] J. Zhao. Determination of optimal build orientation based on satisfactory degree theory for rpt. In *Proceedings - Ninth International Conference on Computer Aided Design and Computer Graphics, CAD/CG 2005 2005, art. no. 1604640*, pages 225–230.

[33] J. Zhao, L. He, W. Liu, and H. Bian. Optimization of part-building orientation for rapid prototyping manufacturing. *Journal of Computer-Aided Design and Computer Graphics*, 18(3):456–463, 2006.

[34] E. Zitzler. *Evolutionary Algorithms for Multiobjective Optimization: Methods and Applications*. PhD thesis, ETH Zurich, Switzerland, 1999.